IEEE Access
Multidisciplinary | Rapid Review | Open Access Journal

Received December 1, 2019, accepted December 12, 2019, date of publication December 17, 2019,
date of current version December 30, 2019.

Digital Object Identifier 10.1109/ACCESS.2019.2960290

Design of Low-Cost BLAC Motors for Integrated Electric Brake Systems

KYU-YUN HWANG[1,2] AND BYUNG-IL KWON[1], (Senior Member, IEEE)
[1]Department of Electronic Engineering, Hanyang University, Ansan 15588, South Korea
[2]Department of IDB PJT Development Team II, Mando, Seongnam 13486, South Korea

Corresponding author: Byung-Il Kwon (bikwon@hanyang.ac.kr)

This work was supported by the Korea Institute of Energy Technology Evaluation and Planning (KETEP) and the Ministry of Trade, Industry & Energy (MOTIE) of the Republic of Korea under Grant 20174030201780, and in part by the BK21PLUS Program through the National Research Foundation of Korea within the Ministry of Education.

ABSTRACT During motor production processes, the influence of motor manufacturing tooling costs on motor prices is mostly negligible and considered to be insignificant. The manufacturing cost, particularly the molding cost, may not be a significant issue for mass production, but it would become a crucial issue for modern small-scale application-oriented design. When the total number of motors produced per motor manufacturing tool such as stator and rotor pressing tool is reduced, the effect of the motor manufacturing tool cost on the motor price can be greatly increased. To reduce the cost, we present a new design approach of a brushless AC (BLAC) motor that shares motor manufacturing tools, unlike many previous studies on low-cost designs. The design approach of a BLAC motor is applied to integrated electric brake (IEB) systems of various specifications. In addition, to analyze the motor performances in IEB systems, the BLAC vector control system, FEM, design of experiment, and moving least square method are used. Furthermore, to predict the available operating time of a motor, a heat compensation coefficient that uses the experimental data of an existing motor is proposed. By implementing this design approach, we have effectively designed motors that satisfy performance requirements such as speed response, available operating time, and total harmonics distortion (THD) of back EMF with minimum stator core volume, in the IEB systems, and achieve a 25.5% reduction in cost through sharing of motor manufacturing tools.

INDEX TERMS Brushless AC motor, integrated electric brake system, manufacturing tools, permanent magnet motor, thermal.

I. INTRODUCTION

Recently, various new parts based on motors have been developed in automobiles and other industrial fields [1], [2]. With the increase in the diversity of motor applications, the performance requirements of motors have also become more diverse. To obtain a more detailed analysis result for the motor behavior, several studies focused on combined research with respect to motor design and control [3], [4]. In addition, various studies on motor design for cost reduction considering various motor characteristics, such as motor torque density, control characteristics, and thermal performance, are being conducted. To reduce costs, studies on reduction of material costs of motors are conducted [5], which includes studies on design methods to minimize magnet consumption by using an efficiency-based optimization technique. Similarly, various studies used a new motor type and winding structure. Methods including use of cost-effective five-phase permanent-magnet vernier machine structure [6], low-cost manufacturing by winding design [7], and high saliency of PMa-SynRM were investigated in previous studies [8]. Furthermore, various motor design methods have been discussed to reduce motor costs [9]–[12], however, very few studies have been conducted on low-cost designs of motors considering the motor manufacturing tools [13], [14]. A method is proposed to significantly improve the reliability and manufacturing quality of the PM soft magnetic composite motor with lower manufacturing condition and cost [13] and a cost-efficient selection of stamping machines for lamination production in the electric traction motor application has been described [14].

The cost of pressing tools for stators and rotor cores as motors manufacturing tools may vary depending on the manufacturing method and process; however, their costs are typically hundreds or thousands of times higher than the material cost of the motor. The pressing tools for stator and rotor cores can be used to manufacture many motors. Furthermore, in most cases, a large number of motors are produced per

The associate editor coordinating the review of this manuscript and approving it for publication was Alfeu J. Sguarezi Filho.

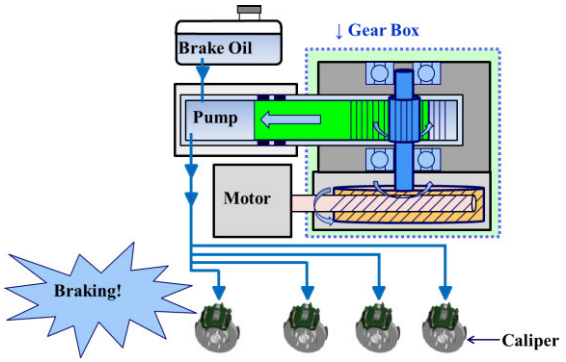

FIGURE 1. Conceptual structure of the IEB systems.

pressing tool; thus, the influence of pressing tools' cost on motor unit cost is negligible. Therefore, most studies dealing with low-cost motor designs are focused on reducing the motor material costs and not motor pressing tools costs. However, in recent years, original equipment manufacturing (OEM) has been demanding diverse cost-competitive products that can satisfy various OEM requirement specifications. Furthermore, if only the requirement specifications are diversified without increasing the total amount, the number of motors produced per manufacturing tool will be reduced and the effect of the pressing tools cost on the motor unit price are also increased. In this case, studies on the pressing tools sharing may be more effective in reducing motor costs than material cost-savings studies. In addition, to produce various types of motors sharing the pressing tools, a multipurpose design that considers the various characteristics of the motors is required. Additionally, one of the most effective ways to reduce the motor cost is to utilize existing experiment data.

In this study, we introduced a design of a low-cost BLAC motor for various integrated electric brake (IEB) systems, which shares motor manufacturing tools to reduce costs and considers the required performance in the IEB systems. The remainder of this paper is organized as follows. In Section II, we introduce the IEB systems. In Section III, we introduce the design of low-cost BLAC motors that share pressing tools for different systems and use existing experiment data of motors. This design consists of six steps. The main points of the proposed design approach are explained progressively.

II. INTEGRATED ELECTRIC BRAKE SYSTEM

Figure 1 shows the conceptual structure of IEB systems. An IEB system mainly consists of a motor, a gear box, and a pump. A brief description of the sequence of operations is as follows: When the driver transmits a signal to the electric control units and an operation signal to the motor, the braking force is transmitted to the vehicle caliper through the gear box and the pump. The motor, which is the main device of the IEB system, must meet all system requirements.

In this study, we introduce a cost-effective motor design approach that meets the various requirements of an IEB system, such as speed response, available operating time, and total harmonics distortion (THD) of the back EMF with

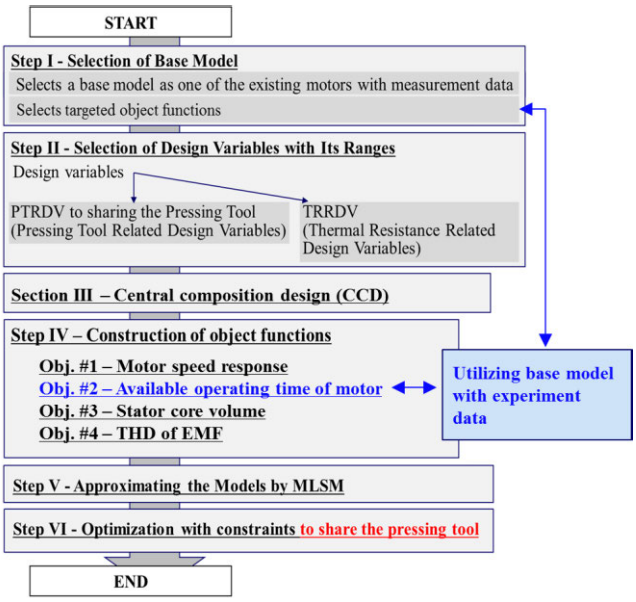

FIGURE 2. Design process of a low-cost BLAC motor.

minimum stator core volume. This will be explained in detail in Section III.

III. DESIGN OF LOW-COST BLAC MOTOR FOR VARIOUS IEB SYSTEMS

The design of a low-cost BLAC motor that shares motor manufacturing tools, such as stator and rotor pressing tools, and uses the experiment data of existing motors for various IEB systems is illustrated in Fig. 2. The design process of a low-cost BLAC motor consists of six steps. First, an existing motor with experimental data is selected as the base model for use in the design of the low-cost BLAC motor. Further, the optimal design is performed. The design variables and objective functions are selected, and the central composite design (CCD) as a design of experiment (DOE) is used to determine the combination for analysis [15]. The moving least square method (MLSM) is used for constructing an approximate model with the selected design variables and objective functions [16]. Finally, using genetic algorithm (GA) and approximated models prepared by MLSM, the constraint optimization design is prepared to share the motor manufacturing tools. It is worth noting that the process of the GA will be conducted using the commercial optimization tool, PIAnO [17].

A. SELECTION OF BASE MODEL (STEP I)

The design process presented in this study begins by selecting an existing motor with experiment data as the base model. Generally, when developing new motors, the industry tries to make the most of the previously developed motors and evaluation data. This is because using an existing motor with experimental data can increase the accuracy of the analysis and reduce the effort required for new motor designs.

For example, when designing a motor with new specifications, an existing motor with experimental

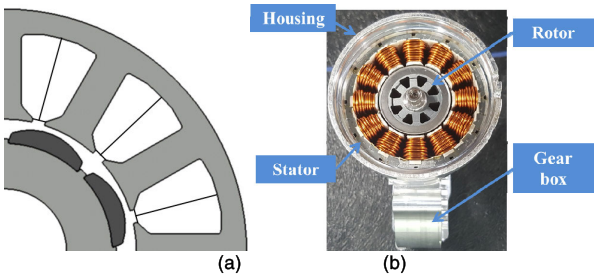

FIGURE 3. (a) Topology and (b) manufactured sample of the base model.

TABLE 1. Specifications of the base model.

Design variables	unit	Base model
Number of phases	-	3
Number of pole pairs and tooth	-	4 / 12
Outer diameter of stator	mm	72
Stack length of stator	mm	34
the structure of the windings	mm	Delta connection 2parallel, 2series per phase
Magnet grade	-	N44UH
Line to line resistance	mΩ	19.5
Max. torque	Nm	3.8
Max. power	W	984

measurement data is selected as the base model and used in the design. The topology and manufactured sample of the selected base model are shown in Fig. 3. The specifications of the base model are listed in Table 1.

Also in the step, we selected targeted objection functions such as motor speed response, available operating time of motor, stator core volume, and THD of EMF. Then the selection of design variables is consider as next step.

B. SELECTION OF DESIGN VARIABLES (STEP II)

After selecting the base model and targeted objection functions, the optimal design is determined. As shown in Fig. 4, the motor design variables of the main performance of the motor are defined, from which the pressing tools-related design variables (PTRDV) and thermal-related design variables (TRRDV) are also chosen. Here, PTRDV and TRRDV are the design variables normally used in the design of stator cores [18] and in thermal equivalent analysis [19], [20], respectively. To estimate the increase in motor coil temperature with varying design variables using the experimental data of the base models, the design variable corresponding to the TRRDV was set at the same value as that of the base model.

In designing a motor, the PTRDV and TRRDV can be selected from the design variables of the main performance of the motor, as shown in Fig. 4. If the same PTRDV are designed, the whole motor unit cost reduction effect is obtained by sharing the pressing tools for the stator and rotor core. Furthermore, if TRRDV is designed to be the same, the thermal resistance condition in the radial direction is the same.

The selected design variables, (X1i, X2i, and X3i) as (⑩, ③, and ⑫) used in the optimal design of the motor, are shown

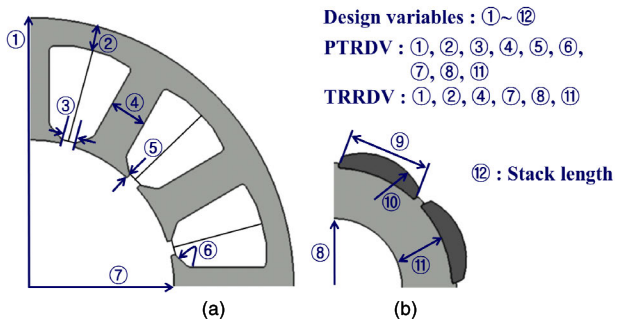

FIGURE 4. PTRDV and TRRDV among the design variables. (a) Stator and (b) rotor.

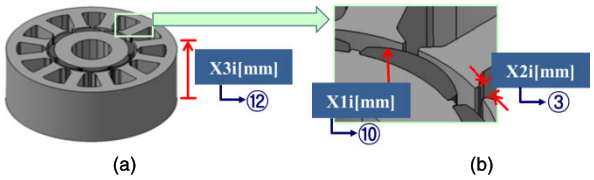

FIGURE 5. Selected design variables of the motor.

TABLE 2. Design variables for CCD.

Design variables	Level of design variables	
	Min.	Max.
X1i [mm]	7.0	12
X2i [mm]	0.5	2.5
X3i [mm]	24	44

in Fig. 5 and presented in Table 2. Even if the number of design variables is less, if at least one PTRDV and TRRDV are included as design variables, the new optimal design approach can be fully explained. The "i" symbol in the design variables represents the system number (System-I, II, and III) with different gearbox specifications. X1i denotes the outer diameter of PM, which does not belong to either PTRDV or TRRDV. X2i denotes the length of the open slot as one of the PTRDV. X3i denotes the stack length of the stator core as one of the TRRDV. In the optimization process, other geometric parameters, except the selected design variables, remain fixed.

Specifically, X2i corresponds to the PTRDV and i corresponds to the system number. When the design variable X2i, which is related to the stator core shape, changes; it belongs to the PTRDV because it is necessary to newly manufacture the pressing tools for the stator core. However, for the design variable X1i, which is related to the permanent magnet shape, the magnet is generally not related to the pressing tools because it is formed by machining and not manufacturing the pressing tools.

C. CCD (STEP III)

In this step, the CCD is performed to obtain the analysis sampling points for the combination of design variables. The CCD is used to estimate the fitted model for each response [21]. The design of the experiment is prepared using the CCD,

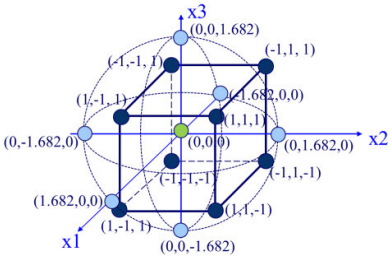

FIGURE 6. CCD with three variables.

TABLE 3. Simulation results for CCD.

No.	x1i[mm]	x2i[mm]	x3i[mm]	X1i[mm]	X2i[mm]	X3i[mm]
1	-1	-1	-1	8.01	0.91	28.05
2	1	-1	-1	10.99	0.91	28.05
3	-1	1	-1	8.01	2.09	28.05
4	1	1	-1	10.99	2.09	28.05
5	-1	-1	1	8.01	0.91	39.95
6	1	-1	1	10.99	0.91	39.95
7	-1	1	1	8.01	2.09	39.95
8	1	1	1	10.99	2.09	39.95
9	-1.682	0	0	7.00	1.50	34.00
10	1.682	0	0	12.00	1.50	34.00
11	0	-1.682	0	9.50	0.50	34.00
12	0	1.682	0	9.50	2.50	34.00
13	0	0	-1.682	9.50	1.50	24.00
14	0	0	1.682	9.50	1.50	44.00
15	0	0	0	9.50	1.50	34.00

which consists of a total of 15 runs, as shown in Fig. 6. The decoded design variables are presented in Table 3.

In Fig. 6, x1i, x2i, and x3i are the coded values of the design variables, and X1i, X2i, and X3i show the actual value of the design variables. In this study, we considered the coded values of the design variables.

D. CONSTRUCTION OF OBJECT FUNCTIONS (STEP IV)

The objective functions Y1–Y4 for the optimal design of the motor in the IEB system are constructed in as follows:

1) MOTOR SPEED RESPONSE (Y1 AS OBJECT FUNCTIONS #1)

To satisfy the quick brake performance of the IEB systems (System-I, II, and III), the speed response of the motor under the brake load conditions is analyzed. In IEB systems, the maximum pressure should be generated between 0 and 0.25 seconds for quick braking. Even under the same pressure conditions, the load torque of the motor can vary depending on the gearbox specifications. For example, if the reduction ratio of the gearbox decreases, the load torque of the motor increases, and the required amount of motor rotation decreases. Moreover, when the reduction ratio increases, the load torque of the motor decreases, and the required amount of motor rotation increases. System-I, II, and III consist of different gear reduction ratio such as 62, 49, and 40, respectively. The system requirement of speed response for each system, i.e., System-I, II, and III, required an average speed of over 6000, 7000, and 8000 rpm, respectively, under load torque conditions, as shown in Fig. 7. The required load torque is determined by the gearbox specification.

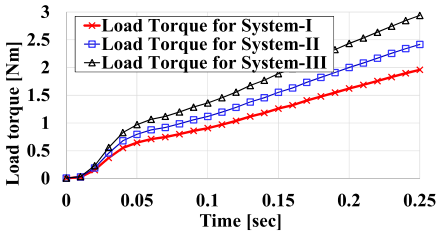

FIGURE 7. Load torque profile for the system I, II, and III.

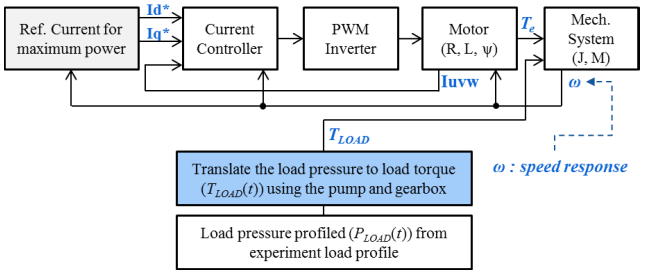

FIGURE 8. Block diagram for calculating the motor speed response in the IEB system.

TABLE 4. Simulation results of speed responses for CCD.

No.	x1i[mm]	x2i[mm]	x3i[mm]	Y1i(i=1)[rpm]	Y1i(i=2)[rpm]	Y1i(i=3)[rpm]
1	-1	-1	-1	8112	6974	5984
2	1	-1	-1	8631	7322	6268
3	-1	1	-1	8886	7625	6557
4	1	1	-1	8997	7794	6665
5	-1	-1	1	7185	6217	5378
6	1	-1	1	7717	6623	5682
7	-1	1	1	8023	6947	6068
8	1	1	1	7999	6986	6120
9	-1.68	0	0	7441	6435	5565
10	1.68	0	0	8579	7415	6458
11	0	-1.68	0	7837	6745	5823
12	0	1.68	0	8475	7386	6450
13	0	0	-1.68	9078	7769	6656
14	0	0	1.68	7679	6579	5637
15	0	0	0	8390	7241	6325

The motor speed response can be analyzed to calculate the average speed under load torque profile in each system by the integration of the BLAC vector control system [22], [23], as shown in Fig. 8.

A 2D FEM is also used to analyze the motor control parameters, such as flux linkage and inductance, considering the nonlinear magnetic saturation characteristics of the core. In this step, the motor average speeds are calculated as the motor speed responses along the CCD. In Table 4, Y1i denotes the motor average speed under 12Vpeak based on the line-to-line voltage and 120°C in the i^{th} system.

2) AVAILABLE OPERATING TIME OF MOTOR USING PROPOSED HEAT COMPENSATION COEFFICIENT (Y2 AS OBJECT FUNCTION #2)

The main motor performance that determines the available operating time for the load driving conditions of the motor is the increase in coil temperature. An accurate estimation of

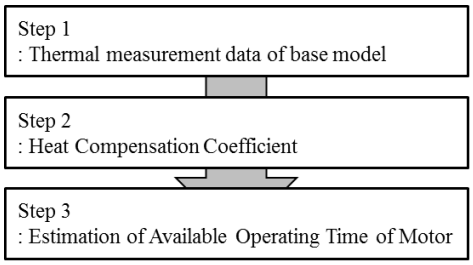

FIGURE 9. Procedure of calculating the available operating time of the motor.

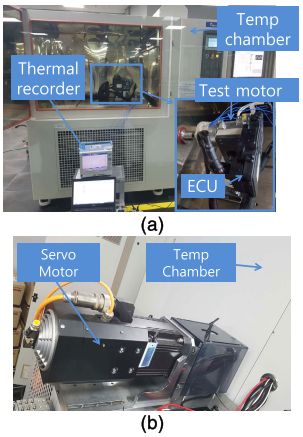

FIGURE 10. Thermal experimental setup. The (a) front and (b) back of the tester chamber back.

the coil temperature is important for calculating the available operating time of the motor. For simple and easy analysis of the motor coil temperatures, the heat compensation coefficients are proposed.

The entire procedure of obtaining the available operating time of the motor is illustrated in Fig. 9. First, we obtain the thermal measurement data of the base model and then use the thermal compensation coefficients to estimate the available operating time of the motor.

- *Thermal measurement data of the base model*

Figure 10 shows the measurement setup used for testing the increase in coil temperature in the motor. To test the thermal characteristics of the base model based on the variation in the ambient temperature under various load conditions, a load test motor is installed in the temperature-variable chamber.

Using the temperature recorder, the temperatures of the coil are measured for each load condition. This can be expressed as the coil temperature variation based on the ambient temperature, as shown in Fig. 11. The ambient temperature condition of the motor to be examined is 120 °C; thus, it was measured at 80 °C to cover the coil variation range more.

- *Proposed Heat Compensation Coefficient*

The measured coil temperature data of the base model (Fig. 10) can be interpolated as expressed as follows:

$$T_C(\boldsymbol{t}) = T_0 + \boldsymbol{f}(\boldsymbol{t}, W_L(\boldsymbol{t})), \tag{1}$$

where T_0 denotes the ambient motor temperature, f(t, $W_L(t)$) is a function of interpolating the increased coil temperature

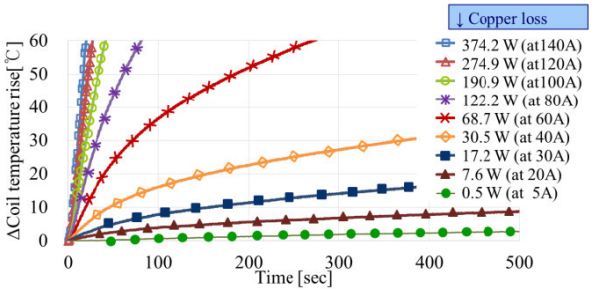

FIGURE 11. Measured coil temperature variation for the copper loss of the base model.

with respect to the ambient temperature using cubic spline interpolation, and $W_L(t)$ denotes the mean cumulative motor loss that is consumed from 0 to t.

In this case, the losses include iron loss, copper loss, and permanent magnet eddy current loss. However, the application is mainly driven at a low speed of about under 1,000rpm in normal braking mode, and is almost at hold when maintaining brake pressure. Therefore, iron loss was ignored, and only copper loss was considered.

The following three assumptions are made to predict the increase in motor coil temperature for the variation in design variables using the experimental data of the base model. First, if the thermal resistance component and the amount of loss are the same, the increase in the motor coil temperature is also the same. Second, the thermal resistance is proportional to the lamination length [24]. Third, the effect of loss and thermal resistance on the increase in motor coil temperature is the same. For example, even if the motor loss increases, the increase in motor coil temperature is the same if the motor thermal resistance increases accordingly. With these three assumptions, to compensate the change in the thermal resistance according to the change in the stator stack lengths, which is a design variable, a heat compensation coefficient, K_H, is proposed as expressed in (2). The purpose of K_H is to use the experimental data of the base model efficiently even if the design variables are changed.

$$K_H = \frac{L'}{L_B} = \frac{R'}{R_B}, \tag{2}$$

where K_H denotes the heat compensation coefficient for the heat transfer dimension in axial variation; L_B and L' denote the stator stack lengths of the base and the redesigned models, respectively; R_B and R' denote the thermal resistances of the base and redesigned models, respectively.

By using the heat compensation coefficient, K_H, and the experimental data of the base model, the increase in coil temperature according to the change in stack length can be predicted as follows:

$$T_C(t) = \boldsymbol{T}_0 + \boldsymbol{f}(\boldsymbol{t}, (1/K_H) \cdot W_L(t)), \tag{3}$$

where $f(t,\ 1/K_H \cdot W_L(t))$ denotes a function to estimate the increase in coil temperature considering the variation in stack length.

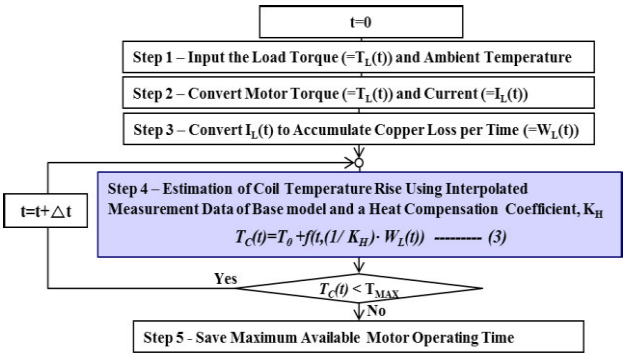

FIGURE 12. Calculation process for available operating time of motor.

However, to simplify the variation in thermal conductivity caused by changes in the design variables versus the base model, the TRRDV that affect the thermal resistance [19] of the motor should not be changed. By using the proposed thermal coefficients and experimental data from the base model, as expressed in (3), the increase in motor coil temperature according to the load driving of the IEB system can be predicted. Further, the estimated increase in motor coil temperature can be used to calculate the available operating time of the motor.

- Estimation of Available Operating Time of Motor

The calculation procedure of the available operating time of the motor according to the driving condition is composed of five steps, as illustrated in Fig. 12.

In step 1, the load operation pattern is the input. In step 2, the consumption current in the motor is calculated according to the load pattern using the motor torque constant as expressed in (4).

$$I_L(t) = T_L(t)/K_t(a1), \tag{4}$$

where $T_L(t)$ is the motor load torque with time, K_t is the torque constant indicating a torque amplitude of a motor per current, and a1 indicates the ambient temperature when the motor is driven.

In step 3, the motor loss due to ambient temperature and load conditions is calculated through integration [26], as expressed in (5). The mean cumulative motor loss values used by the actuation time are calculated as follows:

$$W_L(t_n) = \left(\frac{h}{2} [W_L(t_0) - W_L(t_n)] + h \sum_{i=1}^{n-1} W_L(t_i) \right) \Big/ t_n, \tag{5}$$

where t_0 denotes the start time, t_n denotes the final time, h denotes the time step, n denotes the total number of data points, and $W_L(t)$ denotes the calculated motor loss for the system load conditions per unit time.

In step 4, to estimate the coil temperature for motor loss, the measurement data of the base model are used. The variation in thermal resistance caused by the change in lamination length is compensated by the constant K_H. In step 5, the available operating time of the motor is calculated by determining the time to reach the motor coil maximum limit temperature 160°C, which is including consideration of test error or design margin.

TABLE 5. Simulation result of available operating time for CCD.

No.	x1i[mm]	x2i[mm]	x3i[mm]	Y2i(i=1)[s]	Y2i(i=2)[s]	Y2i(i=3)[s]
1	-1	-1	-1	59.9	32.3	21.2
2	1	-1	-1	75.7	39.2	24.5
3	-1	1	-1	60	32.4	21.2
4	1	1	-1	77.4	39.4	24.6
5	-1	-1	1	281.1	113.3	56.9
6	1	-1	1	399.5	149.7	70.9
7	-1	1	1	283.4	113.5	57
8	1	1	1	407.4	152.3	72.4
9	-1.68	0	0	113.1	52.5	30.9
10	1.68	0	0	190.8	82.4	44.1
11	0	-1.68	0	147.2	65.2	36.8
12	0	1.68	0	154.3	67.7	37.5
13	0	0	-1.68	40.5	24.3	16.3
14	0	0	1.68	596	211.1	95.8
15	0	0	0	160	70.2	39

TABLE 6. Simulation result of stator core volumes for CCD.

No.	x1i[mm]	x2i[mm]	x3i[mm]	Y3i(i=1,2,3) [cm^3]
1	-1	-1	-1	1142
2	1	-1	-1	1142
3	-1	1	-1	1142
4	1	1	-1	1142
5	-1	-1	1	1626
6	1	-1	1	1626
7	-1	1	1	1626
8	1	1	1	1626
9	-1.68	0	0	1384
10	1.68	0	0	1384
11	0	-1.68	0	1384
12	0	1.68	0	1384
13	0	0	-1.68	977
14	0	0	1.68	1791
15	0	0	0	1384

The available operating times of the motor for CCD in the transient state are calculated by determining the time until the coil temperature reaches the coil specification limit from the ambient temperature. In Table 5, Y2i denotes the available operating time under a constant torque condition in the ith system.

3) STATOR CORE VOLUME (Y3 AS OBJECT FUNCTION #3)

The stator core volumes according to the combination of design variables are calculated. To minimize the weight of the motor for each specification, the volume is also included in the objective functions.

Here, the stator core volumes along the CCD are calculated. In Table 6, Y3i denotes the stator core volume for the ith system, where Y3i is determined based on the value of the design variable regardless of the system number i.

4) THD OF EMF (Y4 AS OBJECT FUNCTION #4)

The THD of EMF, as one of the main source for noise and vibration of motor under the sinusoidal current source system, is selected as the objective function. The THD of EMF according to the combination of design variables are

TABLE 7. Simulation result of THD of EMF for CCD.

No.	x1i[mm]	x2i[mm]	x3i[mm]	Y4i(i=1,2,3)[%]
1	-1	-1	-1	0.46
2	1	-1	-1	0.89
3	-1	1	-1	0.66
4	1	1	-1	0.49
5	-1	-1	1	0.46
6	1	-1	1	0.89
7	-1	1	1	0.67
8	1	1	1	0.50
9	-1.68	0	0	0.47
10	1.68	0	0	0.90
11	0	-1.68	0	0.60
12	0	1.68	0	0.60
13	0	0	-1.68	0.48
14	0	0	1.68	0.47
15	0	0	0	0.48

calculated as follows:

$$THD = 100 \cdot \frac{\sqrt{V_2^2 + V_3^2 + V_4^2 + \cdots + V_n^2}}{V_1}, \quad (6)$$

where V_n is the RMS voltage of the n^{th} harmonic and $n = 1$ is the fundamental component.

In Table 7, Y4i denotes the THD of EMF along the CCD for the i^{th} system, where Y4i is determined by the value of the design variable regardless of the system number i.

E. APPROXIMATING THE MODELS BY MLSM (STEP V)

The objective functions Y1–Y4 for the optimal design of the motor in the IEB system are constructed in the following way:

In step V, the MLSM is used as a weighted least square method, wherein each weight depends on the design variables that is approximated. Therefore, the coefficients of the regression model are functions of the design variables. Thus, they must be calculated for each design variable [16].

The following matrix expresses the relationship between the responses and the variables:

$$\boldsymbol{y}' = \beta_0 + \sum_{i=1}^{k} \beta_i \boldsymbol{x_i} + \sum_{i=1, j \le i}^{k} \beta_i \boldsymbol{x_i x_j} + \varepsilon = \boldsymbol{X}\beta + \varepsilon, \quad (7)$$

where y' denotes the vector of the fitted value from the true function y, k is number of design variables, X denotes a matrix of the level of independent variables x_i and x_j, β denotes a vector of the regression coefficients, and ε denotes a vector of random errors.

The least-square function $L_y(x)$ is defined by the following equation, and this expresses the sum of weighted errors as follows:

$$L_y(\boldsymbol{x}) = \sum_{i=1}^{N} W(\boldsymbol{x}) \left(\boldsymbol{y}' - \boldsymbol{y}\right)^2 = W(\boldsymbol{x}) \left(X\beta(\boldsymbol{x}) - \boldsymbol{y}\right)^2, \quad (8)$$

where $W(x)$ denotes a weighting matrix as a function of the location, and this is obtained from the weighting function, y is the simulation results as the known value and N is the number of CCD.

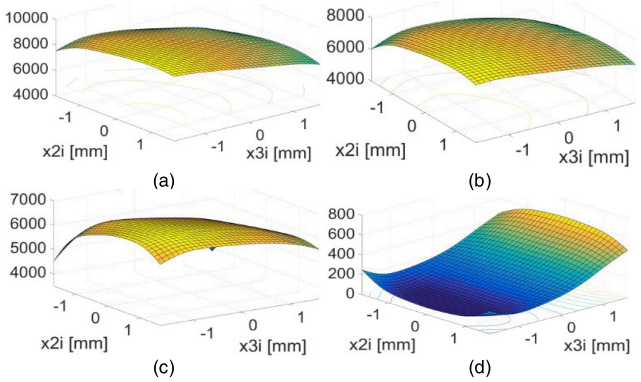

FIGURE 13. Surface plots using MLSM of Y1i, Y2i, and Y3i when x1i = 1. (a) Y1i (i = 1), (b) Y1i (i = 2), (c) Y1i (i = 3), and (d) Y2i (i = 1).

The weighting function $w(x)$ uses the Gaussian function given in (9) as follows:

$$\boldsymbol{w}(\boldsymbol{x}) = \exp\left(-\frac{\boldsymbol{x}^2}{\boldsymbol{h}^2}\right). \quad (9)$$

The weighting matrix $W(x)$ is constructed by using the weighting function $w(x)$ with diagonal terms as follows:

$$W(\boldsymbol{x}) = \begin{bmatrix} \boldsymbol{w}(\boldsymbol{x} - \boldsymbol{x}_1) & 0 & \cdots & 0 \\ 0 & \boldsymbol{w}(\boldsymbol{x} - \boldsymbol{x}_2) & \cdots & 0 \\ \cdots & \cdots & \cdots & \cdots \\ 0 & 0 & \cdots & \boldsymbol{w}(\boldsymbol{x} - \boldsymbol{x}_N) \end{bmatrix}, \quad (10)$$

where x denotes a vector of the approximation location and xi denotes the vector of the i^{th} sampling point.

To minimize $L_y(x)$, the least square estimators must satisfy the following expression:

$$\frac{\partial L_y(\boldsymbol{x})}{\partial \beta(\boldsymbol{x})} = 2X^T \left(W(\boldsymbol{x}) \left(X\beta(\boldsymbol{x}) - \boldsymbol{y}\right)\right) = 0 \; or,$$
$$2X^T \left(W(\boldsymbol{x}) \left(X\beta(\boldsymbol{x})\right)\right) = 2X^T \left(W(\boldsymbol{x})\, y\right) \quad (11)$$

The coefficients of the regressive equation $\beta(x)$ are obtained by the matrix operation as follows:

$$\beta(\boldsymbol{x}) = \left[X^T W(\boldsymbol{x}) X\right]^{-1} X^T W(x)\, y, \quad (12)$$

where the coefficient $\beta(x)$ denotes a function of the position x. It should be noted that the procedure to calculate $\beta(x)$ denotes a local approximation, and the moving processes perform a global approximation throughout the entire design domain.

The surface plots of the object functions and design variables using MLSM are shown in Figs. 13 and 14.

F. OPTIMIZATION WITH CONSTRAINTS TO SHARE THE PRESSING TOOLS FOR STATOR CORE (Step VI)

In step VI, the optimal design is performed to satisfy each system requirements, such as the electromagnetic output, volume, and thermal characteristics of the motor, and the variables related to the pressing tools are included in the constraint function. Furthermore, to compare the optimum design values when considering the sharing of pressing tools

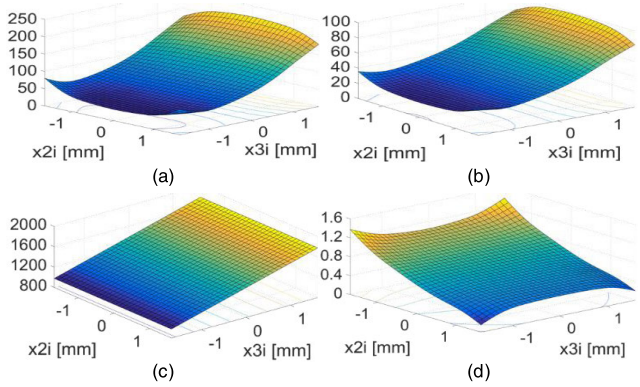

FIGURE 14. Surface plots using MLSM of Y3i and Y4i when x1i = 1. (a) Y2i (i = 2), (b) Y2i (i = 3), (c) Y3i (i = 1,2,3), and (d) Y4i (i = 1,2,3).

and not considering the pressing tools, the optimization design is performed in two cases as follows. Case-I is the optimal design condition considering pressing tools sharing. Case-II is a condition for optimizing the design of each system without considering the common use of pressing tools. Unlike Case-II, in Case-I, the constraint Y5 is included so that even if the system is different, the variable $x2i$ associated with the pressing tools of the stator core has the same value.

$$
\begin{aligned}
&Case-I\\
&\quad Minimize: Y1(x)\ and\ -Y3i(x)\\
&\quad Subject\ to: Y2i(x) < 0.6, 61 < Y4i(x) < 66,\\
&\quad Y5 = \sum_{i=1}^{3}(x2i - m)2 = 0\\
&\quad 7.0 < x1i[mm] < 12.0, 0.5 < x2i[mm] < 2.5,\\
&\quad 24 < x3i[mm] < 44, i = 1, 2, 3\\
&Case-II\\
&\quad Minimize: Y1(x)\ and\ -Y3i(x)\\
&\quad Subject\ to: Y2i(x) < 0.6, 61 < Y4i(x) < 66,\\
&\quad 7.0 < x1i[mm] < 12.0, 0.5 < x2i[mm] < 2.5\\
&\quad 24 < x3i[mm] < 44, i = 1, 2, 3
\end{aligned}
$$

where Y5 is the deviation of the variable $x2i$ related to the pressing tools according to the system I, and m denotes the mean value of all $x2i$ from first to last system.

Figures 14 and 15 show the convergence history plots for the design variables to find the optimal points via MLSM using GA for Case-I and Case-II, respectively.

After conducting the GA-combined modeling technique, MLSM, the optimal values for x1, x2, and x3, which minimize the stator core volume and maximize the motor average speed as well as satisfy the constraint condition for available operating time and THD of the back EMF, are obtained, as presented in Table 8.

G. PERFORMANCE OF OPTIMAL DESIGNED MOTOR

As a result of the optimal design, in Case-I, the values of X2i that corresponds to a design variable is related to the

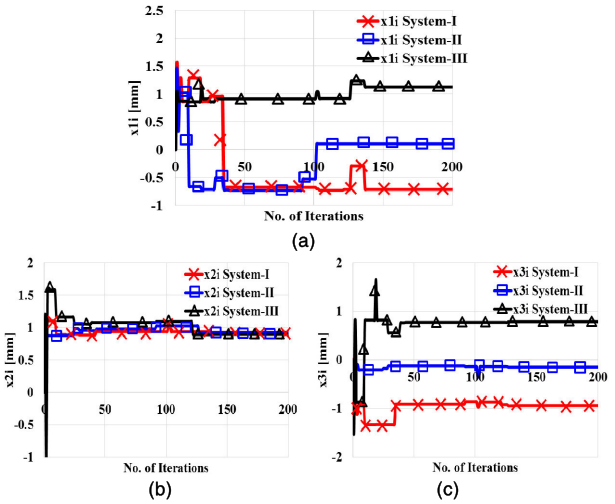

FIGURE 15. Process of searching the optimal design variables for system I, II, and III via GA in Case-I. (a) x1i, (b) x2i, and (c) x3i.

TABLE 8. Optimization results of the design variables.

Items		Design variables		
		x1i[mm]	x2i[mm]	x3i[mm]
Base model for System-II		8.50	1.50	34.00
Case-I	Motor-I for Sys.-I	8.45	2.05	28.42
	Motor-II for Sys.-II	9.66	2.05	33.06
	Motor-III for Sys.-III	11.14	2.03	38.66
Case-II	Motor-I for Sys.-I	8.76	0.80	27.15
	Motor-II for Sys.-II	9.90	1.98	32.81
	Motor-III for Sys.-III	10.31	1.70	38.27

TABLE 9. Optimization results of the object functions.

Items		Objective functions				
		Y1	Y2	Y3	Y4	Y5
Base model for System-II		7105	64.3	1384	0.512	-
Case-I	Motor-I for Sys.-I	8893	65.7	1157	0.597	0.025
	Motor-II for Sys.-II	7467	62.9	1346	0.514	
	Motor-III for Sys.-III	6184	64.9	1574	0.549	
Case-II	Motor-I for Sys.-I	8422	57.2	1105	0.506	-
	Motor-II for Sys.-II	7496	62.6	1335	0.505	-
	Motor-III for Sys.-III	6205	60.0	1558	0.528	-

shape of the stator core and are confirmed to exhibit similar values. There is a minute difference of about 0.01–0.02 mm; however, this is a manufacturing error level and can be ignored. This indicates that the stator core can be composed of the same pressing tool, even if the load conditions required by the system are different. Table 11 presents the optimized design results for Case-I and II.

The estimated coil temperature under the constant load for base model, Case-I, and Case-II are shown in Fig. 17.

To estimate the cost of motors optimized in Case-I and II, the volume and cost per kg information of the main motor components that are listed in Tables 10 and 11 are utilized [24].

The weight of the analytical model is simply calculated using the density and volume of the material. The material cost is calculated using the material volume, density, and cost per kg. Furthermore, the cost of materials is multiplied by

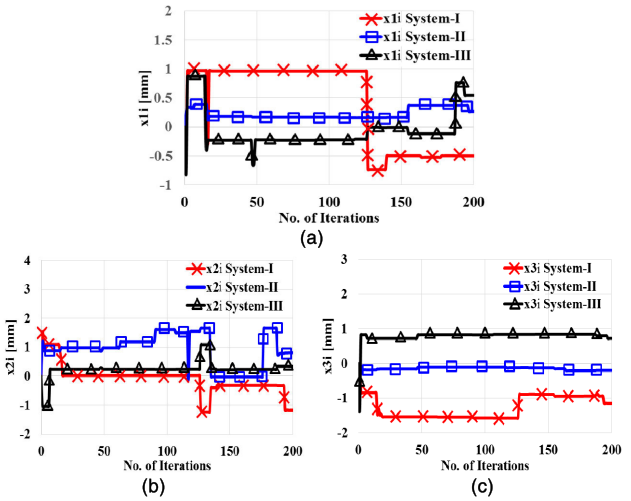

FIGURE 16. Process of searching the optimal design variables for system I, II, and III via GA in Case-II. (a) x1i, (b) x2i, and (c) x3i.

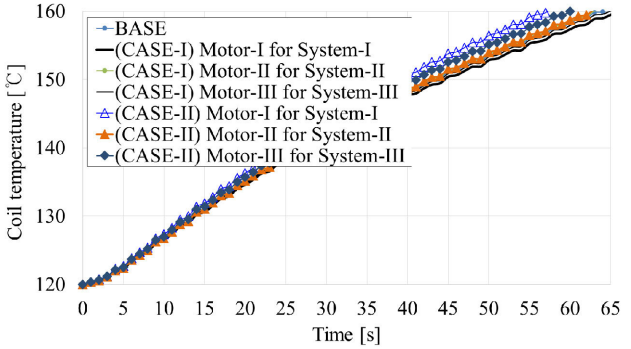

FIGURE 17. Estimated coil temperature under constant load.

TABLE 10. Comparison of volume of main motor component.

Items		Volume [cm^3]		
		Stator core	magnet	coil
Base model for System-II		61.85	6.33	23.14
Case-I	Motor-I for Sys.-I	51.50	5.28	20.41
	Motor-II for Sys.-II	60.10	6.43	22.68
	Motor-III for Sys.-III	70.09	7.81	25.41
Case-II	Motor-I for Sys.-I	49.90	5.11	19.79
	Motor-II for Sys.-II	59.51	6.43	22.55
	Motor-III for Sys.-III	69.62	7.58	25.22

TABLE 11. Materials and tool cost of motor component.

No.	Items	Density	Cost
1	Stator laminations	7.5 g/cm^3	0.0006 [$/g]
2	Magnets (ND)	7.8 g/cm^3	0.075 [$/g]
3	Stator winding (copper)	8.94 g/cm^3	0.0068 [$/g]
4	Stator core pressing tool	-	50,000 [$]

1.4 to account for the scrap rate and machining costs incurred in manufacturing the magnet and core. Here, the value 1.4 is selected based on the experience of the designer.

The material cost (MC) can be expressed as follows:

$$MC = 1.4 \cdot (V_{PM} D_{PM} C_{PM} + V_{ST} D_{ST} C_{ST} + V_{CO} D_{CO} C_{CO}), \tag{13}$$

TABLE 12. Comparison of manufacturing cost of motors in Case-I and II.

Items		Cost		
		MC	TC	Total (=MC+TC)
Base model for System-II		-	-	-
Case-I	Motor-I for Sys.-I	6.38	1.67	8.05
	Motor-II for Sys.-II	7.57	1.67	9.24
	Motor-III for Sys.-III	9.00	1.67	10.67
Case-II	Motor-I for Sys.-I	6.18	5.00	11.18
	Motor-II for Sys.-II	7.56	5.00	12.56
	Motor-III for Sys.-III	8.80	5.00	13.80

where V_{PM}, D_{PM}, and C_{PM} are the volume [cm^3], density [g/cm^3], and cost per g [$/g] of the magnet, respectively. V_{ST}, D_{ST}, and C_{ST} are the volume [cm^3], density [g/cm^3], and cost per g [$/g], of the stator core, respectively. V_{CO}, D_{CO}, and C_{CO} are the volume [cm^3], density [g/cm^3], and cost per g [$/g] of the coil, respectively.

The cost of the pressing tools for the stator core is also obtained based on the experience of the designer of the production. This is because the manufacturing cost of the pressing tools varies depending on the design concept of the designer. Once the tool cost is determined, it is divided by the total production quantity of motor, and this value is reflected in the motor unit price. The tool cost reflected in the motor is given as TC.

$$TC = \frac{C_{\mathrm{tool}}}{PV}, \tag{14}$$

where C_{tool} is the cost [$] of a pressing tool and PV is the total production quantity of the motor.

To compare the motor costs for the optimized results of Case-I and II, the production quantity of each designed motor in systems I, II, and III is assumed to be 10,000 units, which belongs to a small production level. The comparison of manufacturing costs of a motor in Case-I and II are listed in Table 12.

Based on the calculations, the total motor price for Case-I and II is the sum of the total costs of Motor-I, II, and III in each case, which is $27.97 and $37.54, respectively. Case-I shares the manufacturing tools, thereby saving about 25.5% in motor costs as compared to that in Case-II. Furthermore, as the optimal design result, the motor performance in Case-I is similar to that in Case-II; thus, Case-I is selected as the final design.

The speed responses in the different systems are shown in Fig. 18(a) for the base model and optimized motors-I, II, and III. The optimized motor-II exhibits a quick speed response as compared with the base model designed with the same system (System-II). As a result of optimization, it is possible to predict that the thermal characteristics of all motors in systems I, II, and III will be similar even with varying loads because the available operating time of the motor is similar with a constant load. The increase in motor coil temperature in systems I, II, and III are further investigated when the same load pattern was driven in the IEB system, as shown in Fig. 18(b).

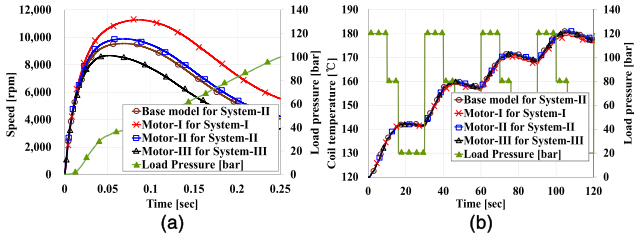

FIGURE 18. Comparison of motor performances. (a) Motor speeds in the quick break mode, (b) Estimated coil temperature.

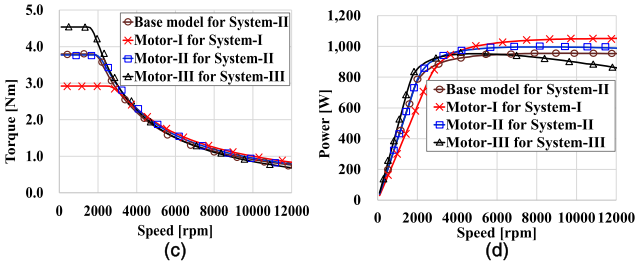

FIGURE 19. Comparison of motor performances with field weakening control. (a) Torque/speed and (b) power/speed.

The torque and power characteristics with respect to the speed of the optimized motor are shown in Fig 19. The results also show that all motors have a wide speed range with field weakening control.

IV. CONCLUSION

In this study, we introduced a design of low-cost BLAC motors for various IEB systems. Using this design, we achieved 25.5% cost reduction through the pressing tools of stator sharing while satisfying the performance requirements in the IEB systems of various specifications.

In motor production, it is relatively less cost-effective to share pressing tools thus, it may be meaningless. However, recent research and development is expected to increase the demand of motors with various specifications because of the increasing number of OEMs and various OEM requirements. Sharing motor manufacturing tools is a simple design concept for low-cost BLAC motors. It can also be applied to brake systems and various systems driven by motors.

In the future work, first, to improve the low-cost design process, the robust design/upgraded optimization will be conducted considering manufacturing error level with the Monte-carlo simulation. Then, the cost of various manufacturing issues with experiment data, which may vary greatly due to many technical and non-technical factors, are also considered. Also, the proposed heat compensation coefficient will be upgrade and applied to the thermal equivalent circuit next study.

REFERENCES

[1] K. M. Rahman, S. Jurkovic, C. Stancu, J. Morgante, and P. J. Savagian, "Design and performance of electrical propulsion system of extended range electric vehicle (EREV) Chevrolet volt," *IEEE Trans. Ind. Appl.*, vol. 51, no. 3, pp. 2479–2488, May/Jun. 2015.

[2] A. Dadashnialehi, A. Bab-Hadiashar, Z. Cao, and R. Hoseinnezhad, "Reliable EMF-sensor-fusion-based antilock braking system for BLDC motor in-wheel electric vehicles," *IEEE Sensors Lett.*, vol. 1, no. 3, Jun. 2017, Art. no. 6000304.

[3] A. Sarikhani and O. A. Mohammed, "Multiobjective design optimization of coupled PM synchronous motor-drive using physics-based modeling approach," *IEEE Trans. Magn.*, vol. 47, no. 5, pp. 1266–1269, May 2011.

[4] E. M. Tsampouris, P. E. Kakosimos, and A. G. Kladas, "Coupled computation of electric motor design and control parameters based on ant colonies speed trajectory optimization," *IEEE Trans. Magn.*, vol. 49, no. 5, pp. 2177–2180, May 2013.

[5] J. Du, X. Wang, and H. Lv, "Optimization of magnet shape based on efficiency map of IPMSM for EVs," *IEEE Trans. Magn.*, vol. 26, no. 7, Oct. 2016, Art. no. 0609807.

[6] G. Xu, G. Liu, M. Chen, X. Du, and M. Xu, "Cost-effective Vernier permanent-magnet machine with high torque performance," *IEEE Trans. Magn.*, vol. 53, no. 11, Nov. 2017, Art. no. 8206104.

[7] R. Wrobel, D. Staton, R. Lock, J. Booker, and D. Drury, "Winding design for minimum power loss and low-cost manufacture in application to fixed-speed PM generator," *IEEE Trans. Ind. Appl.*, vol. 51, no. 5, pp. 3773–3782, Sep./Oct. 2015.

[8] T. A. Huynh and M.-F. Hsieh, "Comparative study of PM-assisted SynRM and IPMSM on constant power speed range for EV applications," *IEEE Trans. Magn.*, vol. 53, no. 11, Nov. 2017, Art. no. 8211006.

[9] A. El-Refaie, T. Raminosoa, P. Reddy, S. Galioto, D. Pan, K. Grace, J. Alexander, and K.-K. Huh, "Comparison of traction motors that reduce or eliminate rare-earth materials," *IET Electr. Syst. Transp.*, vol. 7, no. 3, pp. 207–214, Sep. 2017.

[10] R. Wrobel, N. Simpson, P. H. Mellor, J. Goss, and D. A. Staton, "Design of a brushless PM starter generator for low-cost manufacture and a high-aspect-ratio mechanical space envelope," *IEEE Trans. Ind. Appl.*, vol. 53, no. 2, pp. 1038–1048, Mar. /Apr. 2017.

[11] S. Sashidhar and B. G. Fernandes, "A novel ferrite SMDS spoke-type BLDC motor for PV bore-well submersible water pump," *IEEE Trans. Ind. Appl.*, vol. 64, no. 1, pp. 104–114, Jan. 2017.

[12] B. Ma, G. Lei, J. Zhu, Y. Guo, and C. Liu, "Application-oriented robust design optimization method for batch production of permanent-magnet motors," *IEEE Trans. Ind. Electron.*, vol. 65, no. 2, pp. 1728–1739, Feb. 2018.

[13] G. Lei, J. G. Zhu, Y. G. Guo, J. F. Hu, W. Xu, and K. R. Shao, "Robust design optimization of PM-SMC motors for six sigma quality manufacturing," *IEEE Trans. Magn.*, vol. 49, no. 7, pp. 3953–3956, Jul. 2013.

[14] J. Zhang, D. Spath, Y. He, and A. Boronka, "Cost-efficient selection of stamping machines for lamination production in the electric traction motor application," in *Proc. 8th Int. Electr. Drives Prod. Conf. (EDPC)*, Dec. 2018.

[15] K.-C. Kim, D.-H. Koo, and J. Lee, "The study on the overhang coefficient for permanent magnet machine by experimental design method," *IEEE Trans. Magn.*, vol. 43, no. 6, pp. 2483–2485, Jun. 2007.

[16] K.-Y. Hwang, H. Lin, S.-H. Rhyu, and B.-I. Kwon, "A study on the novel coefficient modeling for a skewed permanent magnet and overhang structure for optimal design of brushless DC motor," *IEEE Trans. Magn.*, vol. 48, no. 5, pp. 1918–1923, May 2012.

[17] *PIAnO Introduction*. Accessed: Apr. 2018. [Online]. Available: http://pidotech.com/en/product/piano.aspx

[18] X. Zhu, B. Yan, L. Chen, R. Zhang, L. Quan, and L. Mo, "Multi-objective optimization design of a magnetic planetary geared permanent magnet brushless machine by combined design of experiments and response surface methods," *IEEE Trans. Magn.*, vol. 50, no. 11, Nov. 2014, Art. no. 8204004.

[19] P. H. Mellor, D. Roberts, and D. R. Turner, "Lumped parameter thermal model for electrical machines of TEFC design," *IEE Proc. B-Electr. Power Appl.*, vol. 138, no. 5, pp. 205–218, Sep. 1991.

[20] C. Sciascera, P. Giangrande, L. Papini, C. Gerada, and M. Galea, "Analytical thermal model for fast stator winding temperature prediction," *IEEE Trans. Ind. Electron.*, vol. 64, no. 8, pp. 6116–6126, Aug. 2017.

[21] H. W. Lee, S. G. Lee, S. H. Won, and J. Lee, "Optimal design of high-precision maglev system using simulation-based DOE and FEM," *IEE Proc.—Electric Power Appl.*, vol. 153, no. 5, pp. 773–779, Sep. 2006.

[22] M. Barcaro, N. Bianchi, and F. Magnussen, "Permanent-magnet optimization in permanent-magnet-assisted synchronous reluctance motor for a wide constant-power speed range," *IEEE Trans. Ind. Electron.*, vol. 59, no. 6, pp. 2495–2502, Jun. 2012.

[23] X. Liu, H. Chen, J. Zhao, and A. Belahcen, "Research on the performances and parameters of interior PMSM used for electric vehicles," *IEEE Trans. Ind. Electron.*, vol. 63, no. 6, pp. 3533–3545, Jun. 2016.
[24] F. Ahmed, E. Ghosh, and N. C. Kar, "Transient thermal analysis of a copper rotor induction motor using a lumped parameter temperature network model," in *Proc. IEEE Transp. Electrific. Conf. Expo (ITEC)*, Jun. 2016, pp. 1–6.
[25] E. A. Grunditz, S. T. Lundmark, M. Alatalo, T. Thiringer, and A. Nordelöf, "Three traction motors with different magnet materials—Influence on cost, losses, vehicle performance, energy use and environmental impact," in *Proc. 13th Int. Conf. Ecolog. Vehicles Renew. Energies (EVER)*, Apr. 2018, pp. 1–13.
[26] C. F. Gerald and P. O. Wheatley, *Applied Numerical Analysis*. Reading, MA, USA: Addison-Wesley, 1998.

KYU-YUN HWANG was born in Seoul, South Korea, in 1983. He received the B.S. degree in electronic and computer engineering from Hanyang University, Ansan, South Korea, in 2005, where he is currently pursuing the Ph.D. degree with the Department of Electronics, Electrical, Control and Instrumentation Engineering.

From 2010 to 2012, he was a Researcher with Komotek Company, Ltd., Sungnam, South Korea. Since 2012, he has been a Researcher with the Department of IDB PJT Development Team II, Mando, Seongnam, South Korea. His research interest includes design, analysis, and optimization of electric machines.

BYUNG-IL KWON was born in 1956. He received the B.S. and M.S. degrees in electrical engineering from Hanyang University, Ansan, South Korea, in 1981 and 1983, respectively, and the Ph.D. degree in electrical engineering, machine analysis from the University of Tokyo, Tokyo, Japan, in 1989.

From 1989 to 2000, he was a Visiting Researcher with the Faculty of Science and Engineering Laboratory, University of Waseda, Tokyo. In 1990, he was a Researcher with the Toshiba System Laboratory, Yokohama, Japan. In 1991, he was a Senior Researcher with the Institute of Machinery and Materials Magnetic Train Business, Daejeon, South Korea. From 2001 to 2008, he was a Visiting Professor with the University of Wisconsin–Madison, Madison, WI, USA. He is currently a Professor with Hanyang University. His research interest includes design and control of electric machines.